Fault Distance Estimation in Multiterminal HVDC Systems using the Lomb-Scargle Periodogram

Vinícius A. Lacerda, Renato M. Monaro, Denis V. Coury

***Abstract*—Multiterminal high-voltage direct current (HVDC) systems still need to be improved in terms of protection to maximize their availability. In this paper, a new distance protection algorithm is proposed. The fault distance is estimated using the frequency of the DC voltage oscillation in fault conditions and the cable travelling wave speed. The frequency is estimated using the Lomb-Scargle Periodogram (LSP). The LSP can calculate a signal spectral power for arbitrary frequency values, which does not need to be an integral multiple of the inverse of the time window. It can also process signals with missing samples, which makes it easier to use in real-world applications when data can be lost in the communication. In the proposed algorithm, only local measurements are used, without communication. The proposed algorithm was tested in a four-terminal multiterminal HVDC system and was fully selective in simulation environment. To further verify the technique's applicability, the proposed algorithm was embedded in a digital signal controller, and was simulated in real-time. In all the tests simulated in hardware, the faults were correctly detected and identified as being internal (zone 1) or external (zone 2). The results highlighted the potential of the Lomb-Scargle Periodogram and indicated that the proposed algorithm could be used in real-world applications, adding selectivity to multiterminal DC protection schemes.**

***Keywords*—Lomb-Scargle Periodogram, MMC, Multiterminal HVDC, Protection, Short-circuits.**

I. Introduction

ONE significant challenge in multiterminal High Voltage Direct Current (HVDC) systems is a selective protection [1]. Short-circuits must be correctly detected and isolated in a few milliseconds, removing the smallest operation area.

Several protection algorithms for transmission lines/cables have been proposed. Travelling wave based algorithms provide high-speed protection and it is immune to power flow variations[2]–[7]. However, it has elevated measurement system requirements and may find it difficult to distinguish the arrival of consecutive wavefronts in case of close-up faults. Moreover, the algorithm may increase in complexity in case of multiple reflections within a multiterminal system. Differential protection is intrinsically selective and highly sensitive but it requires a dedicated communication link and accurate data synchronisation [8], [9]. The dependency on a communication link also reduces the overall reliability of the system. Moreover, the time delay required to ensure reliable operation may become prohibitive in large systems. Derivative-based protection are one of the most promising techniques for MTDC protection. They operate fast and present good selectivity [10]–[13]. However, they may find it challenging to identify a faulty cable/line in case the of a high fault resistance associated with noise. Transient-based and machine learning-based protection, despite presenting a good performance [14]–[18], lacks a simpler and more straightforward design. Finally, alternative schemes based on distributed optical sensors [19], active pulse injection [20] and distance protection [21]–[23] have also been proposed, which shows that fault identification is still an open research topic to new contributions [24].

Among several protection algorithms for transmission lines/cables, distance protection stands out as it is intrinsically related with the nature of the protected element (protection zones are defined in terms of distance), it has lower measurement-system requirements and does not require any communication to operate. However, differently from AC systems, where the distance is estimated using the impedance [25], [26], the lack of a fundamental power frequency in DC systems precludes the estimation of impedance, and consequently the calculation of the distance to the fault based on the estimated impedance. To circumvent this limitation, alternative distance protection algorithms were proposed for HVDC systems [21], [22], [27]–[29].

In this study, the distance is estimated using the frequency of the DC voltage oscillation in fault condition and the cable travelling wave speed. The frequency is estimated using the Lomb-Scargle Periodogram (LSP). The proposed distance protection has the benefit of not requiring communication, as in [3], [4], [15], [30], not requiring additional sensors, as in [31], [32], operating faster than differential equations based methods, as in [27], and having a straightforward setup.

The proposed algorithm was analysed in software and hardware simulations. The algorithm was fully selective for all tested faults, providing a precise fault distance estimation and presenting a better frequency resolution than the Discrete Fourier Transform (DFT).

The remainder of the paper is organised as follows. Section II introduces the relationship between natural frequency and fault distance. Section III briefly introduces the LSP, the core of the proposed algorithm. The complete protection algorithm is presented in Section IV and its performance is evaluated using simulations in Section V. The hardware implementation and further tests in hardware are described in Section VI. Finally, the conclusions are drawn in Section VII.

This work was funded by the São Paulo Research Foundation (FAPESP), grant number [2015/21167-6]. V. A. Lacerda, R. M. Monaro and D. V. Coury are affiliated with the University of São Paulo, Brazil. (e-mail: vinicius.albernaz.freitas@usp.br; monaro@usp.br; coury@sc.usp.br).

Paper submitted to the International Conference on Power Systems Transients (IPST2021) in Belo Horizonte, Brazil June 6-10, 2021.

II. Relating Natural Frequency and Distance

When a fault happens in an HVDC system, the DC voltage is suddenly reduced at the fault spot, which generates travelling waves in both cable directions. Considering that cable characteristic impedance is greater than short-circuit resistance and is smaller than the converter equivalent impedance, reflections at the converter terminal maintain the polarity, while reflections at the fault point change the wave polarity. As the polarity is inverted only at the fault point and a wave period consists of two polarity changes, four travelling wave periods are needed to form a complete DC voltage oscillation. This concept is illustrated in the lattice diagram in Fig. 1, where Γ_A and Γ_F are the reflection coefficients of point A and F, respectively. For the sake of simplicity, only the reflections between the fault (point *F*) and the converter *A* were considered.

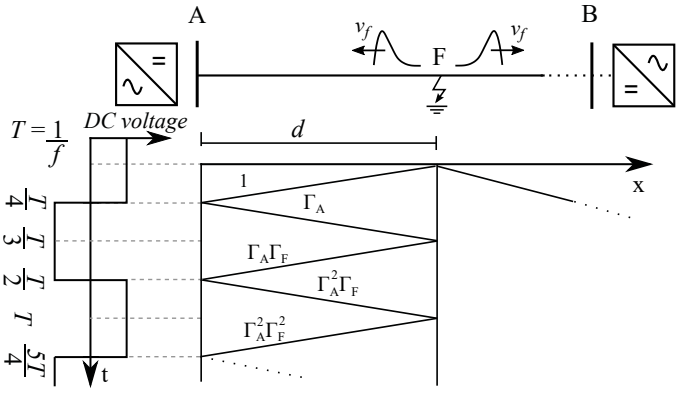

Fig. 1. Lattice diagram.

Therefore, the voltage frequency (f) can be related to distance (d) using the travelling wave speed in the given frequency (ν_f):

$$d = \frac{\nu_f}{4\,f} \tag{1}$$

As shown in Fig. 1, the greater the distance between the fault and the converter, the longer the time elapsed before the reflected wave reaches the measuring terminal and the more spaced the oscillations of the DC voltage become. Therefore, if the frequency of the DC voltage could be calculated, it would be possible to estimate the fault distance and then locate the fault within a primary or secondary protection zone.

However, estimating f in a DC system is not simple given that f is dependent on the distance and that the DC voltage waveform during the fault is formed by multiple reflections and an exponential decay. Therefore, using frequency estimation techniques as the DFT may result in a poor estimation. Additionally, as the frequency is not known beforehand, DC offset removal techniques as in [33] cannot be used. Thus, in order to provide a more precise frequency estimation, the Lomb-Scargle Periodogram (LSP) was used. The characteristics of the LSP are discussed in the next section.

III. The Lomb-Scargle Periodogram

The LSP was developed by N. R. Lomb [34] and J. D. Scargle [35]. Despite being less known in the Power & Energy (P&E) field, the LSP has been widely used in the Astronomical field due to its capacity to test the significance of weak periodic signals and process unevenly sampled data [36], [37]. The LSP can be calculated as follows [37]:

Given a time series x_i, $i = 1, 2, N$ at respective observation times t_i (not necessary evenly spaced), the first step is to calculate the signal's mean ($\bar{x}$) and variance (σ^2) within the window of size N:

$$\bar{x} = \frac{1}{N}\sum_{i=1}^{N} x_i \tag{2}$$

$$\sigma^2 = \frac{1}{N-1}\sum_{i=1}^{N}(x_i - \bar{x})^2 \tag{3}$$

The second step is to define the required set of angular frequencies ω. These angular frequencies do not need to be related with the sampling window as the DFT. Moreover, this set can be composed of as many frequencies of interest as required.

Next, a time-offset τ is calculated for each ω to ensure time-shift invariance:

$$\tau = \frac{1}{2\omega}\tan^{-1}\left(\frac{\sum_{i=1}^{N}\sin(2\omega t_i)}{\sum_{i=1}^{N}\cos(2\omega t_i)}\right) \tag{4}$$

Finally, the Lomb-Scargle periodogram is calculated as

$$P_N(\omega) = \frac{1}{2\sigma^2}\left(\frac{\left(\sum_i^N (x(t_i)-\bar{x})\cos\omega(t_i-\tau)\right)^2}{\sum_i^N \cos^2\omega(t_i-\tau)} + \frac{\left(\sum_i^N (x(t_i)-\bar{x})\sin\omega(t_i-\tau)\right)^2}{\sum_i^N \sin^2\omega(t_i-\tau)}\right) \tag{5}$$

where, $P_N(\omega)$ is the normalized periodogram (spectral power as function of ω).

Differently from the DFT, where the window size defines the frequency of the calculated harmonics, in the LSP the spectral power is calculated for every desired frequency, which does not need to be an integral multiple of the inverse of the time window. Therefore, the LSP can reveal if a signal's power is concentrated around a specified frequency value, rather than only at fixed harmonics as the DFT. Therefore, as the fault distance estimation depends on the precision of the dominant frequency estimation, as shown in (1), the LSP can greatly contribute to revealing the dominant natural frequency.

An interesting property of the LSP is that it is motivated by the Fourier analysis, but it can be viewed as a least-squares method [37], [38]. Another important feature of the LSP is its capacity of processing signals with missing samples, which makes it easier to use in real-world applications when data can be lost in the communication. The differences between LSP and DFT and a more detailed explanation of the LSP can be found in [38].

IV. Proposed Protection Algorithm

The proposed protection algorithm uses the DC voltage oscillation frequency to estimate the fault distance, using (1). As each peak in the LSP indicates the presence of a frequency component, the frequency where the greatest peak occurs is used in (1). As $P_N(\omega)$ in (5) is calculated for every desired frequency, a limited set of frequency values should be selected. One possible solution would be to define a minimum frequency value, a maximum frequency value and a frequency step and evaluate $P_N(\omega)$ for all frequencies within this range and step. The greatest value in $P_N(\omega)$ would indicate the signal's dominant frequency. However, as the fault signal can have frequencies from a few hundreds of Hz to several kHz, small frequency steps would require hundreds of calculations. To overcome this, a top-down procedure is adopted: first, a more spaced set of frequencies is evaluated and the frequency in which $P_N(\omega)$ has the greatest value is selected. Then, a new set of frequencies less-spaced around the previous frequency is evaluated. This step is repeated until the required frequency precision is reached. This procedure is depicted in Fig. 2.

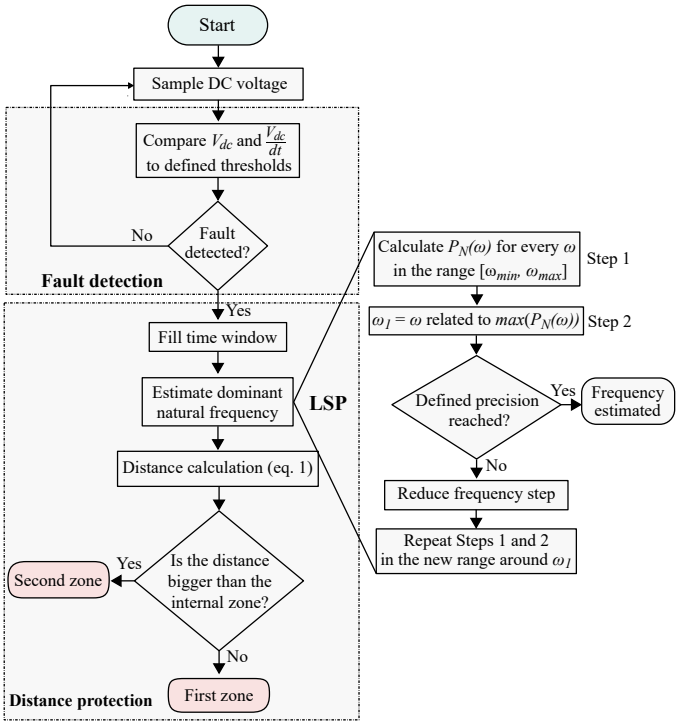

Fig. 2. Proposed distance protection algorithm.

In this study, three iterations of LSP were considered. The first iteration started with a frequency range of 100 Hz to 5000 Hz in steps of 100 Hz. The second was around the greatest frequency obtained in the first step but in smaller steps of 10 Hz. The third was around the greatest frequency in the second step but in smaller steps of 1 Hz. Therefore, the dominant frequency was estimated with a precision of 1 Hz.

The time-window used in the LSP is formed after fault detection. The size of the time window must be chosen according to the maximum time allowed by the DC circuit breaker supportability and by the length of the protected line/cable. For example, in the system presented in Fig. 3, the length of Link 24 is 150 km. As the travelling wave speed in the cables is 183.5 km/ms, the travelling wave delay is 0.818 ms for 150 km. Hence, it takes $4 \cdot 0.818 = 3.27$ ms to form one period in the voltage oscillation if a fault happens at the end of the protected cable. Thus, the window length was chosen as 3 ms, which ensures that 90% of the first zone is covered. This means that for distant faults the algorithm would process an incomplete period, impacting its performance. Choosing a wider window would improve the accuracy but would allow less time for circuit breaker operation.

As the positive- and negative-poles terminal voltages are the only variables used in the proposed protection algorithm, and as the LSP is not sensitive to noise, the measurements provided by existing voltage transducers at each system terminal can be used in the proposed scheme.

In this paper it was also considered that between two measurement points only one type of conductor would be used. If overhead lines are used in conjunction with underground or submarine cables, new challenges arise and the method must be adapted to consider this specificity. Regarding AC faults, as the proposed algorithm is triggered only in case of undervoltage with large voltage derivative, we can assume that only DC faults would trigger the fault identification algorithm.

V. Simulation Results

The system presented in Fig. 3 was simulated using the parameters summarised in Table III, in the Annex. The circuit breaker responsible for the protection of Link 24 (DCB 24) as taken as a reference. The system was modelled in PSCAD/EMTDC and its parameters were based on [39]. The converters were modelled with the detailed Thévenin equivalent model. All DC links were modelled using the frequency-dependent cable model. The DC reactor L_{dc} was 30 mH for MMCs 1, 2 and 3 and 50 mH for MMC 4. L_{bus} was 10 mH for all MMCs.

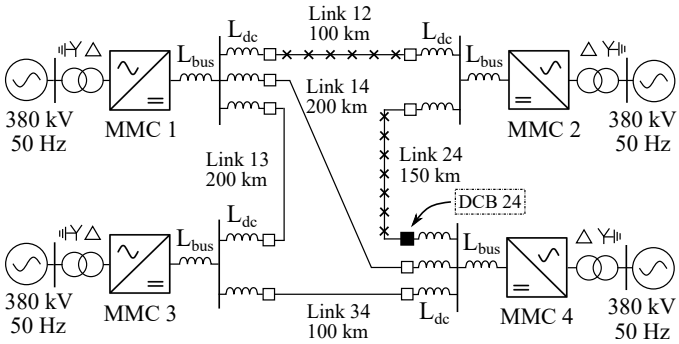

Fig. 3. MTDC test system used for the algorithm evaluation.

The fault detection was made using combined criteria of undervoltage (0.80 p.u) and voltage derivative (0.2 pu/ms). The sampling frequency was 25 kHz. Lower sampling frequencies up to 10 kHz were also tested with similar results.

In the short-circuit simulation, 1 Ω pole-to-pole faults were applied to Link 24 from 10 km to 140 km and to Link 12

from 10 km to 90 km. Gaussian noise was introduced in the generated signals, with SNR of 45 dB.

Figure 4 depicts the frequency estimation performed by the LSP for a 1 Ω fault 40 km from MMC4. As can be observed in Fig. 4 , the frequency estimation gets more precise after each iteration, when converging to the peak value. The final estimated frequency was around 1192 Hz, which using (1) resulted in a estimated distance of 38.5 km, very close to the true value..

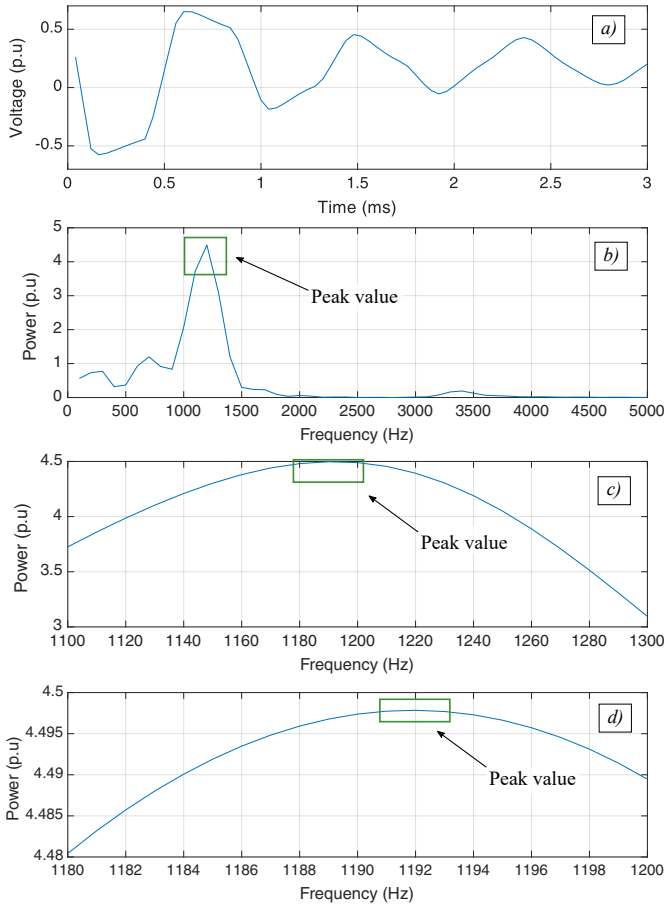

Fig. 4. Example of LSP frequency estimation. a) voltage signal. b) first iteration of frequency estimation with 100 Hz step. c) second iteration with 10 Hz step. d) third iteration with an 1 Hz step.

Table I summarizes the algorithm performance for the tested cases. It can be observed from Table I that the protection algorithm was fully selective, distinguishing between faults inside and outside the protection zone. The distance was estimated with an average error of 1.78 % and a maximum error of 5.91 %. It can also be observed that only a few Hz separate the first to the second zone, which underscores the challenge of the selective operation. When substituting the LSP by the DFT using the Fast Fourier Transform (FFT) algorithm (Table II), this tenuous border between the first and second zone produced higher errors (average error of 7.07 % and maximum error of 25.08 %) and led to incorrect operations when the fault happened outside the protected link, which underscores the advantage of LSP over FFT in this case. As the FFT is a discrete-time sequence with equal spacing in frequency [40], a narrow time-window produces a wide spectrum with low precision in the frequency domain[41].

TABLE I
DISTANCE ESTIMATION USING THE LOMB-SCARGLE PERIODOGRAM.

Link	Fault location	Estimated frequency	Estimated distance	Error %	Zone	Correct operation
Link 24	10 km	4511 Hz	10.2 km	0.11	1st zone	✓
	20 km	2272 Hz	20.2 km	0.13	1st zone	✓
	30 km	1529 Hz	30.0 km	0.002	1st zone	✓
	40 km	1199 Hz	38.3 km	1.16	1st zone	✓
	50 km	823 Hz	55.7 km	3.83	1st zone	✓
	60 km	730 Hz	62.8 km	1.89	1st zone	✓
	70 km	646 Hz	71.0 km	0.68	1st zone	✓
	80 km	578 Hz	79.4 km	0.42	1st zone	✓
	90 km	515 Hz	89.1 km	0.61	1st zone	✓
	100 km	460 Hz	99.7 km	0.18	1st zone	✓
	110 km	432 Hz	106.2 km	2.54	1st zone	✓
	120 km	356 Hz	128.9 km	5.91	1st zone	✓
	130 km	367 Hz	125.0 km	3.33	1st zone	✓
	140 km	343 Hz	133.8 km	4.17	1st zone	✓
Link 12	150 + 10 km	301 Hz	152.41 km	-	2nd zone	✓
	150 + 20 km	296 Hz	155.0 km	-	2nd zone	✓
	150 + 30 km	298 Hz	153.9 km	-	2nd zone	✓
	150 + 40 km	295 Hz	155.5 km	-	2nd zone	✓
	150 + 50 km	296 Hz	155.0 km	-	2nd zone	✓
	150 + 60 km	286 Hz	160.4 km	-	2nd zone	✓
	150 + 70 km	293 Hz	156.6 km	-	2nd zone	✓
	150 + 80 km	206 Hz	222.7 km	-	2nd zone	✓
	150 + 90 km	100 Hz	458.8 km	-	2nd zone	✓

TABLE II
DISTANCE ESTIMATION USING THE FFT.

Link	Fault location	Estimated frequency	Estimated distance	Error %	Zone	Correct operation
Link 24	10 km	4333 Hz	10.6 km	0.39	1st zone	✓
	20 km	2333 Hz	19.7 km	0.23	1st zone	✓
	30 km	1667 Hz	27.5 km	1.65	1st zone	✓
	40 km	1333 Hz	34.4 km	3.73	1st zone	✓
	50 km	1000 Hz	45.9 km	2.75	1st zone	✓
	60 km	667 Hz	68.8 km	5.88	1st zone	✓
	70 km	667 Hz	68.8 km	0.79	1st zone	✓
	80 km	667 Hz	68.8 km	7.46	1st zone	✓
	90 km	667 Hz	68.8 km	14.13	1st zone	✓
	100 km	333 Hz	137.6 km	25.08	1st zone	✓
	110 km	333 Hz	137.6 km	18.42	1st zone	✓
	120 km	333 Hz	137.6 km	11.75	1st zone	✓
	130 km	333 Hz	137.6 km	5.08	1st zone	✓
	140 km	333 Hz	137.6 km	1.58	1st zone	✓
Link 12	150 + 10 km	333 Hz	137.6 km	-	2nd zone	✗
	150 + 20 km	333 Hz	137.6 km	-	2nd zone	✗
	150 + 30 km	333 Hz	137.6 km	-	2nd zone	✗
	150 + 40 km	333 Hz	137.6 km	-	2nd zone	✗
	150 + 50 km	333 Hz	137.6 km	-	2nd zone	✗
	150 + 60 km	333 Hz	137.6 km	-	2nd zone	✗
	150 + 70 km	333 Hz	137.6 km	-	2nd zone	✗
	150 + 80 km	333 Hz	137.6 km	-	2nd zone	✗
	150 + 90 km	333 Hz	137.6 km	-	2nd zone	✗

The average processing time for the LSP and for the FFT in Table I and Table II was 693.3 μs and 48.9 μs, respectively. The tests were performed in a DELL XPS 8500, with 12GB of RAM and with an Intel(R) Core(TM) i7-3770 CPU 3.40GHz, quad-core processor.

When the fault resistance increases, the travelling waves are more attenuated and the LSP performance is affected, as

shown in Fig. 5. However, as can be observed in Fig. 5, the algorithm showed appropriate selectivity for the first protection zone even for higher fault resistances.

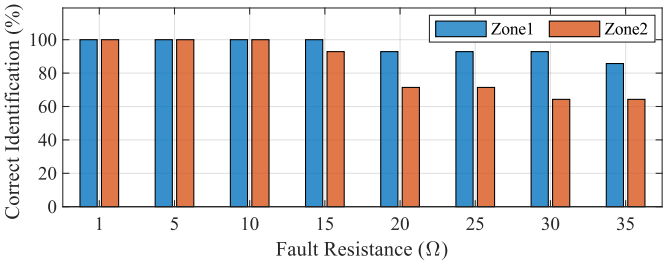

Fig. 5. Influence of fault resistance on the algorithm performance (protection reach).

VI. Real-Time Simulation

In order to verify the applicability of the proposed technique, the complete algorithm was embedded and tested in hardware running in real-time. The algorithm was embedded in a TMS320F28379D Dual-Core Delfino™ Digital Signal Controller (DSC) from Texas Instruments. The DSC pins were accessed through a TMDSDOCK28379D Experimenter Kit. The algorithm ran at a sampling frequency of 25 kHz. A 12-bit Analog-to-Digital Converter (ADC) was used to sample the DC voltage, providing a resolution of 4096 levels.

The fault waveforms simulated in PSCAD were loaded in a Digilent Analog Discovery 2 oscilloscope/signal generator and then injected into the DSC. The waveforms were converted to analog voltage signals between 0–3 V, using the scale -260 kV (-0.81 p.u) equivalent to 0 V and 320 kV (1.0 p.u) equivalent to 3 V. -260 kV and 320 kV were the minimum and maximum values obtained in the simulations. The same oscilloscope was used to read the digital outputs from the DSC, containing the protection trips, distance estimation and the LSP processing time. The calculated distance was displayed in the digital output in the following way: a DSC pin was set at high during a time interval proportional to the estimated distance (0.1 ms per km).

As the oscilloscope is controlled by PC, the fault waveforms were generated after a trigger was received. The trigger was generated using one of the oscilloscopes' digital outputs, commanded by PC. The triggered operation ensured that the generated waveforms were synchronised and that the test start time could be known.

The exchanged signals between the oscilloscope and the DSC are depicted in Fig. 6 and the experiment setup is presented in Fig. 7.

Besides the intrinsic noise present in the process of generating the waveforms and converting to digital values, an additional Gaussian noise was introduced in the generated signals, with SNR of 45 dB, in order to test the algorithm robustness. After conversion, the DC voltage was filtered by a moving average filter of four samples.

The first test was an internal fault 60 km from the DCB 24. Fig. 8 shows the captured window of the DC voltage waveform after fault detection. The window width was 3 ms according to the design presented in Section IV. The algorithm elapsed

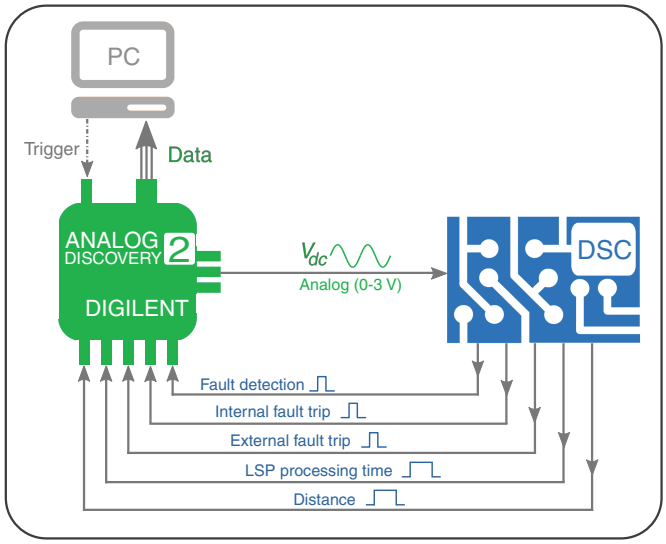

Fig. 6. Experiment schematic diagram.

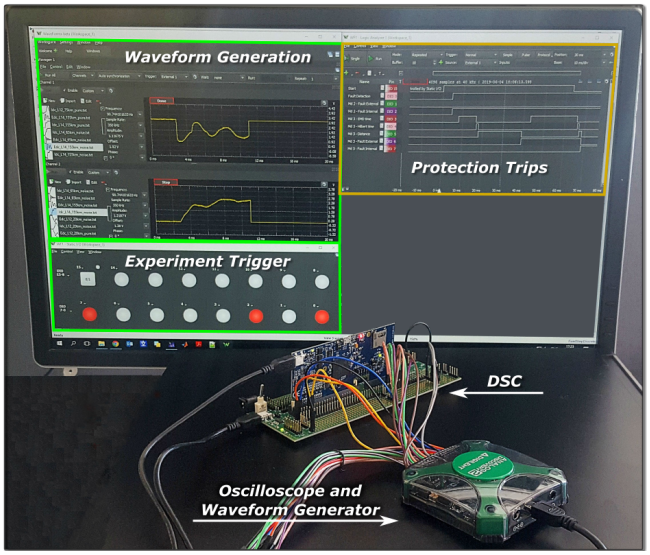

Fig. 7. Experiment setup.

time and protection trips are shown in Fig. 9. After a few milliseconds of pre-fault signal, the fault was detected. The fault detection trip started the distance algorithm and the LSP estimated the frequency. The estimated frequency was multiplied by the travelling wave speed resulting in a distance of 61.5 km (6.15 ms of pulse width). As the calculated distance was smaller than the cable length, the fault was correctly identified as internal (first protection zone).

The second test was an external fault at Link 12, 20 km after the end of Link 24. Fig. 10 shows the captured window of the DC voltage waveform after fault detection. The protection trips are shown in Fig. 11. The estimated distance was 158.5 km (15.85 ms of pulse width). As the calculated distance was greater than the cable length, the fault was correctly identified as external (second protection zone).

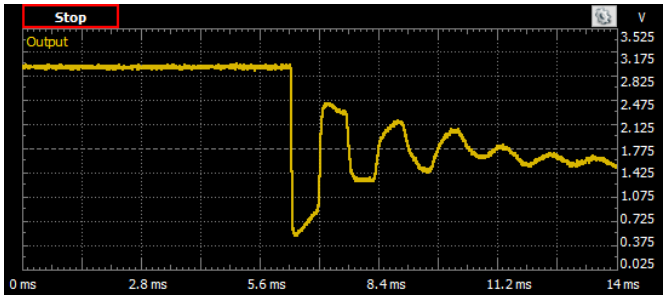

Fig. 8. Analog DC voltage waveform. Fault at Link 24, 60 km from DCB 24.

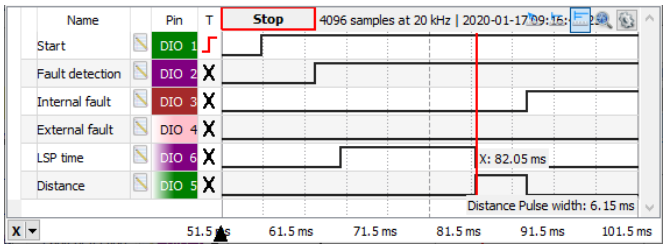

Fig. 9. Protection triggers. Fault at Link 24, 60 km from DCB 24.

VII. Conclusions

Fast and selective protection of HVDC systems is necessary to provide reliable operation of modern multiterminal configurations. In this context, distance protection can play a major role, providing the required selectivity for fault detection algorithms.

In this study, a distance protection algorithm based on natural frequency estimation is proposed. The distance is estimated using the frequency of the DC voltage oscillation in fault condition and the cable travelling wave speed. The frequency is estimated using the LSP. The algorithm does not require communication, it has a simple setup and fast operation. The LSP presented improved frequency resolution compared to the FFT, it was fully selective either in a software simulation environment and hardware simulation and provided a precise frequency estimation.

Although the distance to the fault is estimated by the proposed algorithm, the primary purpose of the distance protection algorithm is to use the estimated distance to quickly protect the lines/cables in fault, without any communication, and not to locate the fault. For fault location, precise algorithms that may require communication might be used.

The results highlight the potential of signal processing techniques in distance protection algorithms and indicated that the proposed algorithm could be used in real-world applications, adding selectivity to multiterminal DC protection schemes.

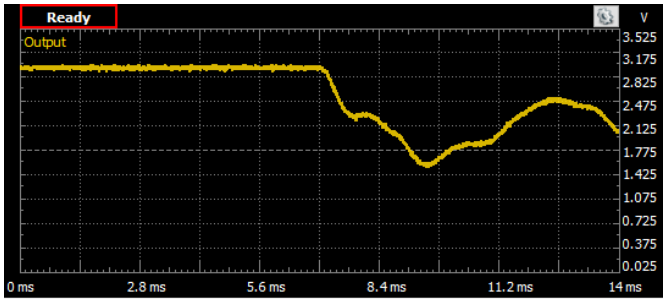

Fig. 10. Analog DC voltage waveform. Fault at Link 12, 20 km after the end of Link 24.

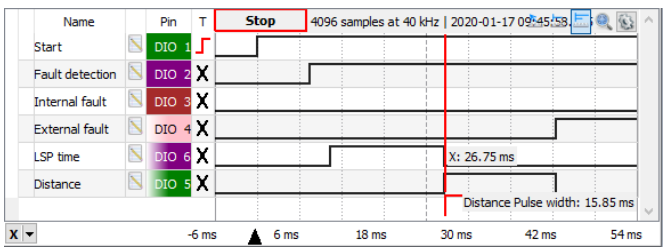

Fig. 11. Protection triggers. Fault at Link 12, 20 km after the end of Link 24.

VIII. Acknowledgements

The authors would like to acknowledge the University of São Paulo, São Carlos, Brazil for the facilities provided. We would also like to thank the São Paulo Research Foundation (FAPESP), grant number [2015/21167-6] for funding this research.

IX. Annex

The test system parameters are summarised in Table III.

TABLE III
Test system parameters.

	MMC 1,2,3	MMC 4	
AC grid			
Voltage	380	380	(kV)
Frequency	50	50	(Hz)
AC reactance	17.75	13.34	(Ω)
AC resistance	1.77	1.34	(Ω)
Transformer			
Nominal power	900	1200	(MVA)
Leakage reactance	0.15	0.15	(p.u.)
Transformer relation	400/400	400/400	(kV/kV)
Connection	Y-g/D	Y-g/D	
Converter			
Nominal voltage	380	380	(kV)
Nominal power	900	1200	(MVA)
Number of SMs per arm	50	50	
Submodule capacitance	1465	1950	(μF)
Arm inductance	84.8	63.6	(mH)
SM ON-state resistance	0.0177	0.0134	(Ω)
SM OFF-state resistance	100	100	(MΩ)
DC bus			
Smoothing reactor (L_{bus})	10	10	(mH)
DC capacitor (C_{bus})	2.5	2.5	(μF)
DC reactor (L_{dc})	30	50	(mH)

References

[1] D. Jovcic and K. Ahmed, *High voltage direct current transmission: converters, systems and DC grids*. John Wiley & Sons, 2015.

[2] J. Wang, B. Berggren, K. Linden, J. Pan, and R. Nuqui, "Multi-terminal dc system line protection requirement and high speed protection solutions," in *Across Borders–VDC Systems and Market Integration*. Lund: CIGRE, 2015.

[3] G. Zou, Q. Feng, Q. Huang, C. Sun, and H. Gao, "A fast protection scheme for VSC based multi-terminal DC grid," *International Journal of Electrical Power & Energy Systems*, vol. 98, pp. 307–314, jun 2018.

[4] Y. Li, Y. Gong, and B. Jiang, "A novel traveling-wave-based directional protection scheme for MTDC grid with inductive DC terminal," *Electric Power Systems Research*, vol. 157, pp. 83–92, apr 2018.

[5] N. Tong, X. Lin, Y. Li, Z. Hu, N. Jin, F. Wei, and Z. Li, "Local measurement-based ultra-high-speed main protection for long distance VSC-MTDC," *IEEE Transactions on Power Delivery*, vol. 34, no. 1, pp. 353–364, feb 2019.

[6] N. Tong, X. Lin, C. Li, Q. Sui, L. Chen, Z. Wang, N. Jin, and Z. Li, "Permissive pilot protection adaptive to DC fault interruption for VSC-MTDC," *International Journal of Electrical Power & Energy Systems*, vol. 123, p. 106234, dec 2020.

[7] Z. Li, Y. Ye, N. Tong, X. Lin, C. Li, N. Jin, and L. Chen, "High error-tolerable unit protection for VSC-MTDC independent of data synchronization," *International Journal of Electrical Power & Energy Systems*, vol. 124, p. 106393, jan 2021.

[8] A. E. Abu-Elanien, A. A. Elserougi, A. S. Abdel-Khalik, A. M. Massoud, and S. Ahmed, "A differential protection technique for multi-terminal HVDC," *Electric Power Systems Research*, vol. 130, pp. 78–88, jan 2016.

[9] M. Elgeziry, M. Elsadd, N. Elkalashy, T. Kawady, A.-M. Taalab, and M. A. Izzularab, "Non-pilot protection scheme for multi-terminal VSC–HVDC transmission systems," *IET Renewable Power Generation*, vol. 13, no. 16, pp. 3033–3042, nov 2019.

[10] J. Sneath and A. D. Rajapakse, "Fault detection and interruption in an earthed HVDC grid using ROCOV and hybrid DC breakers," *IEEE Transactions on Power Delivery*, vol. 31, no. 3, pp. 973–981, jun 2016.

[11] W. Leterme, J. Beerten, and D. V. Hertem, "Nonunit protection of HVDC grids with inductive DC cable termination," *IEEE Transactions on Power Delivery*, vol. 31, no. 2, pp. 820–828, apr 2016.

[12] G. Auran, J. Descloux, S. Nguefeu, and B. Raison, "Non-unit full selective protection algorithm for MTDC grids," in *2017 IEEE Power & Energy Society General Meeting*. Chicago, IL, USA, jul 2017.

[13] Y. M. Yeap, N. Geddada, and A. Ukil, "Capacitive discharge based transient analysis with fault detection methodology in DC system," *International Journal of Electrical Power & Energy Systems*, vol. 97, pp. 127–137, apr 2018.

[14] R. B. Junior, V. A. Lacerda, R. M. Monaro, J. C. M. Vieira, and D. V. Coury, "Selective non-unit protection technique for multiterminal VSC-HVDC grids," *IEEE Transactions on Power Delivery*, pp. 1–1, 2017.

[15] Q. Yang, S. L. Blond, R. Aggarwal, Y. Wang, and J. Li, "New ANN method for multi-terminal HVDC protection relaying," *Electric Power Systems Research*, vol. 148, pp. 192–201, jul 2017.

[16] P. Zhao, Q. Chen, and K. Sun, "A novel protection method for VSC-MTDC cable based on the transient DC current using the s transform," *International Journal of Electrical Power & Energy Systems*, vol. 97, pp. 299–308, apr 2018.

[17] W. Xiang, S. Yang, and J. Wen, "ANN-based robust DC fault protection algorithm for MMC high-voltage direct current grids," *IET Renewable Power Generation*, vol. 14, no. 2, pp. 199–210, dec 2019.

[18] Y. Li, L. Wu, J. Li, L. Xiong, X. Zhang, G. Song, and Z. Xu, "DC fault detection in MTDC systems based on transient high frequency of current," *IEEE Transactions on Power Delivery*, vol. 34, no. 3, pp. 950–962, jun 2019.

[19] D. Tzelepis, A. Dysko, G. Fusiek, J. Nelson, P. Niewczas, D. Vozikis, P. Orr, N. Gordon, and C. D. Booth, "Single-ended differential protection in MTDC networks using optical sensors," *IEEE Transactions on Power Delivery*, vol. 32, no. 3, pp. 1605–1615, jun 2017.

[20] G. Song, T. Wang, and K. S. Hussain, "DC line fault identification based on pulse injection from hybrid HVDC breaker," *IEEE Transactions on Power Delivery*, vol. 34, no. 1, pp. 271–280, feb 2019.

[21] J. Yang, J. E. Fletcher, and J. O'Reilly, "Multiterminal DC wind farm collection grid internal fault analysis and protection design," *IEEE Transactions on Power Delivery*, vol. 25, no. 4, pp. 2308–2318, oct 2010.

[22] P. Tunnerhoff, C. Petino, M. Battiato, and A. Schnettler, "Distance protection for HVDC transmission lines based on MMC modulation strategy," in *2016 Electric Power Quality and Supply Reliability (PQ)*. IEEE, aug 2016.

[23] V. A. Lacerda, R. M. Monaro, D. Campos-Gaona, D. V. Coury, and O. Anaya-Lara, "Distance protection algorithm for multiterminal HVDC systems using the hilbert–huang transform," *IET Generation, Transmission & Distribution*, vol. 14, no. 15, pp. 3022–3032, aug 2020.

[24] CIGRE Working Group B4-52, *Technical Brochure 533: HVDC Grid Feasibility Study*. CIGRE, 2013.

[25] C. Christopoulos and A. Wright, *Electrical Power System Protection*. Springer US, 1999.

[26] S. H. Horowitz and A. G. Phadke, *Power System Relaying*. John Wiley & Sons, Ltd, apr 2008.

[27] J. Suonan, J. Zhang, Z. Jiao, L. Yang, and G. Song, "Distance protection for HVDC transmission lines considering frequency-dependent parameters," *IEEE Transactions on Power Delivery*, vol. 28, no. 2, pp. 723–732, apr 2013.

[28] Z. He, K. Liao, X. Li, S. Lin, J. Yang, and R. Mai, "Natural frequency-based line fault location in HVDC lines," *IEEE Transactions on Power Delivery*, vol. 29, no. 2, pp. 851–859, apr 2014.

[29] V. A. Lacerda, R. M. Monaro, D. Campos-Gaona, D. V. Coury, and O. Anaya-Lara, "Distance protection algorithm for multiterminal HVDC systems using the hilbert–huang transform," *IET Generation, Transmission & Distribution*, vol. 14, no. 15, pp. 3022–3032, aug 2020.

[30] Q. Huang, G. Zou, S. Zhang, and H. Gao, "A pilot protection scheme of DC lines for multi-terminal HVDC grid," *IEEE Transactions on Power Delivery*, vol. 34, no. 5, pp. 1957–1966, oct 2019.

[31] W. Leterme and D. V. Hertem, "Cable protection in HVDC grids employing distributed sensors and proactive HVDC breakers," *IEEE Transactions on Power Delivery*, vol. 33, no. 4, pp. 1981–1990, aug 2018.

[32] R. Ara, U. A. Khan, A. I. Bhatti, and B. W. Lee, "A reliable protection scheme for fast DC fault clearance in a VSC-based meshed MTDC grid," *IEEE Access*, vol. 8, pp. 88 188–88 199, 2020.

[33] Y. Guo, M. Kezunovic, and D. Chen, "Simplified algorithms for removal of the effect of exponentially decaying DC-offset on the fourier algorithm," *IEEE Transactions on Power Delivery*, vol. 18, no. 3, pp. 711–717, jul 2003.

[34] N. R. Lomb, "Least-squares frequency analysis of unequally spaced data," *Astrophysics and Space Science*, vol. 39, no. 2, pp. 447–462, feb 1976.

[35] J. D. Scargle, "Studies in astronomical time series analysis. II - statistical aspects of spectral analysis of unevenly spaced data," *The Astrophysical Journal*, vol. 263, p. 835, dec 1982.

[36] J. H. Horne and S. L. Baliunas, "A prescription for period analysis of unevenly sampled time series," *The Astrophysical Journal*, vol. 302, p. 757, mar 1986.

[37] W. H. Press and G. B. Rybicki, "Fast algorithm for spectral analysis of unevenly sampled data," *The Astrophysical Journal*, vol. 338, p. 277, mar 1989.

[38] J. T. VanderPlas, "Understanding the lomb–scargle periodogram," *The Astrophysical Journal Supplement Series*, vol. 236, no. 1, p. 16, may 2018.

[39] W. Leterme, N. Ahmed, D. V. Hertem, J. Beerten, S. Norrga, and L. Ängquist, "A new HVDC grid test system for HVDC grid dynamics and protection studies in EMT-type software," in *11th IET International Conference on AC and DC Power Transmission*. Institution of Engineering and Technology, 2015.

[40] K. D. Rao and M. Swamy, *Digital Signal Processing*. Springer Singapore, 2018.

[41] A. Moukadem, D. O. Abdeslam, and A. Dieterlen, *Time-Frequency Domain for Segmentation and Classification of Non-Stationary Signals*. John Wiley & Sons, Inc., feb 2014.